

## Polarized photon measurements of the $^{12}\text{C}(\vec{\gamma},pp)$ and $^{12}\text{C}(\vec{\gamma},pn)$ reactions for $E_\gamma=160-350$ MeV

C. J. Y. Powrie,<sup>1</sup> J. C. McGeorge,<sup>1</sup> I. J. D. MacGregor,<sup>1</sup> J. Ahrens,<sup>4</sup> J. R. M. Annand,<sup>1</sup> J. F. Arneil,<sup>2</sup> R. Beck,<sup>4</sup>  
D. Branford,<sup>1</sup> S. Franczuk,<sup>1</sup> D. I. Glazier,<sup>1</sup> P. Grabmayr,<sup>1</sup> S. J. Hall,<sup>1</sup> T. Hehl,<sup>3</sup> P. D. Harty,<sup>1</sup> D. G. Ireland,<sup>1</sup> J. D. Kellie,<sup>1</sup>  
K. Livingston,<sup>1</sup> F. A. Natter,<sup>3</sup> S. Oberkirsch,<sup>3</sup> R. O. Owens,<sup>1</sup> J. Ryckebusch,<sup>5</sup> M. Sauer,<sup>3</sup> A. Settele,<sup>3</sup> and D. P. Watts<sup>1</sup>

<sup>1</sup>*Department of Physics and Astronomy, University of Glasgow, Glasgow G12 8QQ, United Kingdom*

<sup>2</sup>*Department of Physics and Astronomy, University of Edinburgh, Edinburgh EH9 3JZ, United Kingdom*

<sup>3</sup>*Physikalisches Institut, Universität Tübingen, D-72076 Tübingen, Germany*

<sup>4</sup>*Institut für Kernphysik, Universität Mainz, D-55099 Mainz, Germany*

<sup>5</sup>*Department of Subatomic and Radiation Physics, University of Gent, Proeftuinstraat 86, B-9000 Gent, Belgium*

(Received 6 April 2001; published 1 August 2001)

The  $^{12}\text{C}(\vec{\gamma},pp)$  and  $^{12}\text{C}(\vec{\gamma},pn)$  reactions have been studied for  $E_\gamma=160-350$  MeV using linearly polarized photons from the Glasgow tagged photon spectrometer at the Mainz microtron MAMI. Both reaction channels show a negative photon asymmetry  $\Sigma$  for missing energies  $E_m$  below 70 MeV, where direct emission nucleon pairs is expected. A strong peak at low  $E_m$  is observed in  $\Sigma_{(\gamma,pp)}$ , but not in  $\Sigma_{(\gamma,pn)}$ . Further differences between the two reaction channels are observed in the  $E_\gamma$  dependence of  $\Sigma$  and in the angular distributions of differential cross sections for photons polarized parallel, or perpendicular, to the reaction plane. Theoretical calculations using an unfactorized distorted wave treatment of direct two-nucleon emission do not agree with the magnitude of the photon asymmetry or the angular dependence of the differential cross sections for either channel. For  $E_m > 70$  MeV and  $E_\gamma > 250$  MeV,  $\Sigma$  has a substantial negative value which is similar for both reaction channels. This is attributed to two-step reactions following initial quasifree pion production.

DOI: 10.1103/PhysRevC.64.034602

PACS number(s): 24.70.+s, 25.20.Lj, 27.20.+n

### I. INTRODUCTION

Measurements of photonuclear reactions using polarized photons provide unique access to observables which are sensitive to the details of the reaction process [1–4]. Cross sections for reactions in which the polarization of the incident photon is either parallel ( $\sigma_{\parallel}$ ) or perpendicular ( $\sigma_{\perp}$ ) to the reaction plane, have different sensitivity to the various possible reaction mechanisms and the photon asymmetry ( $\Sigma$ ), defined by  $\Sigma = (\sigma_{\parallel} - \sigma_{\perp}) / (\sigma_{\parallel} + \sigma_{\perp})$ , emphasizes the differences between  $\sigma_{\parallel}$  and  $\sigma_{\perp}$ .

The unpolarized cross section is proportional to the transverse structure function  $W_T = W^{xx} + W^{yy}$ , which gives an average of the parallel and perpendicular nuclear response, whereas the photon asymmetry can access the differences contained in  $W_{TT} = W^{xx} - W^{yy}$  through the relation  $\Sigma = -W_{TT}/W_T$  [1].  $W_{TT}$  is particularly sensitive to spin variables in the nuclear currents and also to interference between the contributing currents [2]. Measurements of polarization observables therefore provide sensitive tests of models of two-nucleon photoemission reactions.

The  $(\gamma,pn)$  reaction proceeds mainly through  $\Delta$  currents and mechanisms involving meson exchange currents (MEC) [3,2]. Central short range correlations (SRC) and tensor correlations provide a possible means of ejecting a proton-neutron pair via one-body currents, but their contribution is generally predicted to be modest. In contrast, for  $(\gamma,pp)$  reactions, the charge exchange terms of the two-body currents are suppressed, leaving  $\Delta$  currents and SRC. The contribution of the magnetic dipole  $NN \leftrightarrow N\Delta$  transition, for  $^1S_0$  knockout is strongly suppressed in this channel due to angular momentum and parity conservation rules [5]. Experimen-

tal evidence of a significant contribution from the knockout of  $P$ -wave pairs is provided by detailed fits to  $^{12}\text{C}(\gamma,pp)$  missing momentum ( $P_m$ ) spectra [6]. Although SRC are relatively stronger in the  $(\gamma,pp)$  channel, their effects are generally thought to be small in photoreactions below  $\sim 500$  MeV [3]. The calculations reported in Ref. [2] also came to the same conclusion.

Polarized photon measurements provide a unique tool to investigate differences between the two reaction channels. One question of particular interest is the possibility that a significant fraction of the small  $(\gamma,pp)$  cross section could arise from initial  $(\gamma,pn)$  reactions followed by charge exchange final state interactions (FSI). These would be expected to result in a value of  $\Sigma_{(\gamma,pp)}$  with a smaller magnitude than  $\Sigma_{(\gamma,pn)}$ . For low missing energies ( $E_m$ ) FSI processes cannot remove much energy from the two emitted nucleons and tend to remove the same proportion of strength from  $\sigma_{\parallel}$  and  $\sigma_{\perp}$ . Any reduction in  $\Sigma$  is therefore likely to arise from soft scattering of the outgoing nucleons and is not expected to be large. Hence measurements of  $\Sigma$  provide a reasonably clean signal from the initial processes.

There have been several previous measurements of  $(\vec{\gamma},NN)$  reactions in light nuclei. Polarized photon measurements on  $^3\text{He}$  have been carried out at LEGS [7], averaged over the wide photon energy range 235–305 MeV. Strong differences are seen between the  $^3\text{He}(\vec{\gamma},pn)$  and  $(\vec{\gamma},pp)$  reactions with  $\Sigma_{(\gamma,pn)} \sim -0.2$  whereas the  $\Sigma_{(\gamma,pp)}$  has a much smaller value  $\sim -0.05$ . Calculations which include contributions from one-body, two-body, and three-body photon absorption give a good description of the data. They suggest that one- and two-body terms are dominant in the  $(\vec{\gamma},pn)$

reaction while three-body terms dominate in  $(\vec{\gamma}, pp)$ .

Photon asymmetry measurements of the  ${}^4\text{He}(\vec{\gamma}, pn)$  and  ${}^6\text{Li}(\vec{\gamma}, pn)$  reactions have been made at the Yerevan 3.5 GeV electron synchrotron [8]. The  ${}^6\text{Li}$  data spanned photon energies 300–900 MeV and the  ${}^4\text{He}$  data were in the range 450–550 MeV. The data obtained had limited kinematic coverage and were averaged over a wide range of  $E_m$ . Although the  $\Sigma$  values obtained for both  ${}^6\text{Li}$  and  ${}^4\text{He}$  have slightly smaller magnitudes than deuterium data, they have a similar photon energy dependence.

Measurements of  $\Sigma_{(\gamma, pp)}$  and  $\Sigma_{(\gamma, pn)}$  on  ${}^{16}\text{O}$  have been carried out at LEGS in coplanar kinematics with symmetric detection angles for  $E_\gamma = 245\text{--}315$  MeV [9,10]. Reactions in these kinematics depend strongly on  $\Delta$  currents and have little sensitivity to SRC. For  $E_m < 50$  MeV, where direct photon absorption on proton pairs is expected, a result of  $\Sigma_{(\gamma, pp)} \sim -0.3$  was obtained. This is far smaller than the  $-1.0$  expected for a pure  ${}^1S_0$  interaction in coplanar kinematics [3,11] and is interpreted as evidence for the knockout of nucleon pairs from higher relative angular momentum states. For  $E_m < 70$  MeV,  $\Sigma_{(\gamma, pp)}$  is a factor of  $\sim 2$  greater than  $\Sigma_{(\gamma, pn)}$ , indicating fundamental differences in the two reaction channels at low  $E_m$ . However for  $E_m > 70$  MeV  $\Sigma_{(\gamma, pp)}$  and  $\Sigma_{(\gamma, pn)}$  are similar at  $\sim -0.1$ . Valencia model calculations of  ${}^{12}\text{C}(\gamma, NN)$  cross sections [12,13] show that little strength from direct processes persists at high  $E_m$  and reactions involving intermediate pion production become the largest contributor to both charge channels.

More recent  ${}^{16}\text{O}(\vec{\gamma}, pn)$  data obtained for  $(1p)^2$  emission in quasideuteron kinematics, is reported for  $E_\gamma = 210\text{--}330$  MeV [14]. These kinematics are directly comparable with the present work and the  ${}^{16}\text{O}$  data have similar magnitudes to the present  ${}^{12}\text{C} \Sigma_{(\gamma, pn)}$  data [15].

This paper describes measurements of the photon asymmetry of the  $(\vec{\gamma}, pn)$  and  $(\vec{\gamma}, pp)$  reactions on  ${}^{12}\text{C}$  in the  $\Delta$ -resonance region largely using events selected to emphasize the direct two-nucleon emission process. The experiment was designed to give a sufficiently good  $E_m$  resolution to allow the selection of events in which nucleon pairs are emitted from  $(1p)^2$  and  $(1p)(1s)$  orbitals. Measurements are reported for  $E_\gamma = 160\text{--}350$  MeV and the data are compared with calculations of direct two-nucleon emission carried out using the model developed by the Gent theory group [3].

Some first  $\Sigma_{(\gamma, pn)}$  results from  ${}^{12}\text{C}$  have already been published [15]. These showed that for nucleons ejected from  $(1p)^2$  orbitals,  $\Sigma$  is similar to data obtained in other light nuclei, although some of these measurements include a much wider range of  $E_m$ . The  ${}^{12}\text{C}(\vec{\gamma}, pn)$  data also showed a small but systematic reduction in the magnitude of  $\Sigma$  compared to the  ${}^2\text{H}(\vec{\gamma}, pn)$  reaction. The  $\Sigma_{(\gamma, pn)}$  data for the ejection of nucleons from  $(1p)(1s)$  orbitals have a similar magnitude to the  $(1p)^2$  data but a different  $E_\gamma$  dependence. The present paper reports a more detailed analysis of the data, using different data analysis cuts and an improved calculation of the photon polarization  $P$ . The new polarization calculations, discussed below, give slightly larger  $P$  values than previ-

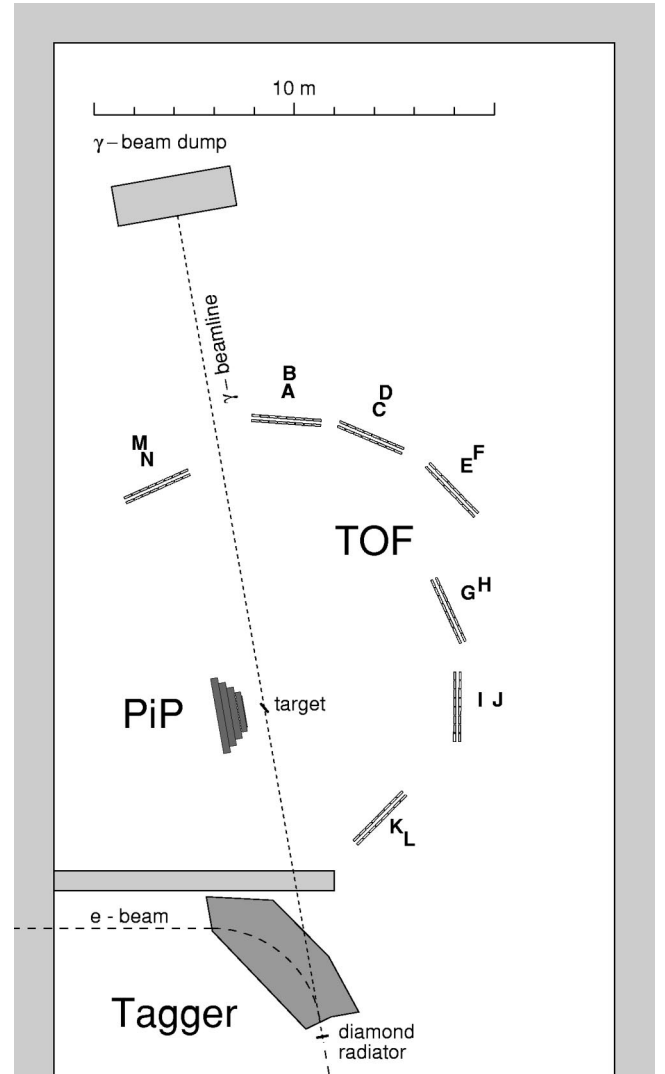


FIG. 1. Schematic diagram of the experimental apparatus.

ously, resulting in  $\Sigma_{(\gamma, pn)}$  values which are reduced in magnitude by  $\sim 6\%$ . This has a small effect on the interpretation of the data previously presented, slightly increasing the difference between the  $\Sigma_{(\gamma, pn)}$  values for  ${}^{12}\text{C}$  and  ${}^2\text{H}$ .

## II. EXPERIMENT

The experiment was carried out using the Glasgow tagged photon spectrometer [16] at the 855 MeV electron accelerator MAMI [17], with a photon energy resolution of  $\sim 2$  MeV. The experimental layout is shown in Fig. 1. A  $100\ \mu\text{m}$  thick, low-mosaic diamond radiator was used to produce coherent bremsstrahlung [18]. The diamond was mounted in a precision goniometer and the crystal was oriented so that the recoil momentum pancake of the bremsstrahlung process, for a selected photon energy, contained the  $[02\bar{2}]$  reciprocal lattice vector. The photon beam was collimated to a half angle of  $0.6$  mrad to select the part of the bremsstrahlung angular distribution which has the highest polarization. Three separate goniometer settings were used to cover the range  $E_\gamma = 160\text{--}350$  MeV and the plane of polarization was rotated

through  $90^\circ$  every few minutes to minimize systematic errors.

The polarized photons were incident on a  $0.5 \text{ g/cm}^2$  graphite target inclined at  $30^\circ$  to the photon beam. Additional calibration data from the  ${}^2\text{H}(\gamma, pn)$  reaction were taken with a  $0.3 \text{ g/cm}^2$   $\text{CD}_2$  target mounted at the same angle.

Protons were detected in PiP [19], a  $\sim 1$  sr plastic scintillation hodoscope covering polar angles from  $50^\circ$  to  $130^\circ$  and azimuthal angles  $-22^\circ$  to  $22^\circ$ . A half-ring of 1 mm thick scintillators [20] (not shown in Fig. 1), placed at a radius of  $\sim 100$  mm round the target, provided a fast trigger and restricted the acceptance to particles produced close to the target. The useful proton energy range of PiP was 31–330 MeV, although very few protons above 200 MeV contributed to the analyzed data. The fraction of protons lost due to inelastic reactions in the scintillator material was calculated using a GEANT Monte Carlo simulation [19] and varied from  $\sim 1.5\%$  at 31 MeV to  $\sim 25\%$  at 200 MeV. These losses were corrected by assigning a weight to each event. Random coincidences between PiP and the tagger, which contributed  $\sim 16\%$  of the measured yield, were subtracted from the final spectra using a sample of purely random events.

Correlated protons and neutrons were detected in TOF [21], an array of plastic scintillator detectors used to measure particle energies by time of flight. TOF scintillator bars (20 cm wide  $\times$  5 cm thick  $\times$  3 m high) were mounted on stands 8 bars wide, 2 layers deep. Using two layers of TOF scintillators increases the neutron detection efficiency and adding the pulse amplitude signals from both layers together permits a clean separation of protons of energies up to 170 MeV from charged pions.

The TOF stands covered a wide range of polar angles as shown in Fig. 1. A half-ring of 2 mm thick scintillators  $\sim 100$  mm from the target on the TOF side of the photon beam, and a second ring at  $\sim 300$  mm [20], were used to distinguish charged and neutral particles. The TOF pulse height thresholds used in the data analysis were chosen to reduce random background without greatly reducing detection efficiency. For neutrons these were set at 17 MeV (9 MeV $_{ee}$ ) which gave an average neutron detection efficiency of  $\sim 9\%$ , calculated using the STANTON code [22], for the double layer of detectors. For protons the effective threshold corresponded to  $\sim 40$  MeV at the target after taking account of energy losses along the proton flight path. Losses of protons in TOF due to inelastic reactions were estimated to be  $\sim 3\%$ , averaged over all proton energies. During the experiment the gains of the TOF PM tubes were monitored using a system of light emitting diodes. Over the whole data taking period the gains were found to vary by less than 2%. For neutrons,  $\sim 15\%$  of the measured yield came from random coincidences. A correction for this was made using a suitably weighted sample of random events from outside the flight-time window. The more stringent particle identification conditions for protons in TOF resulted in a random contribution of less than 1%. This was sufficiently small that no random subtraction was applied in the data analysis.

Contributions from events not originating in the target were measured in a series of target-out runs. The target-out

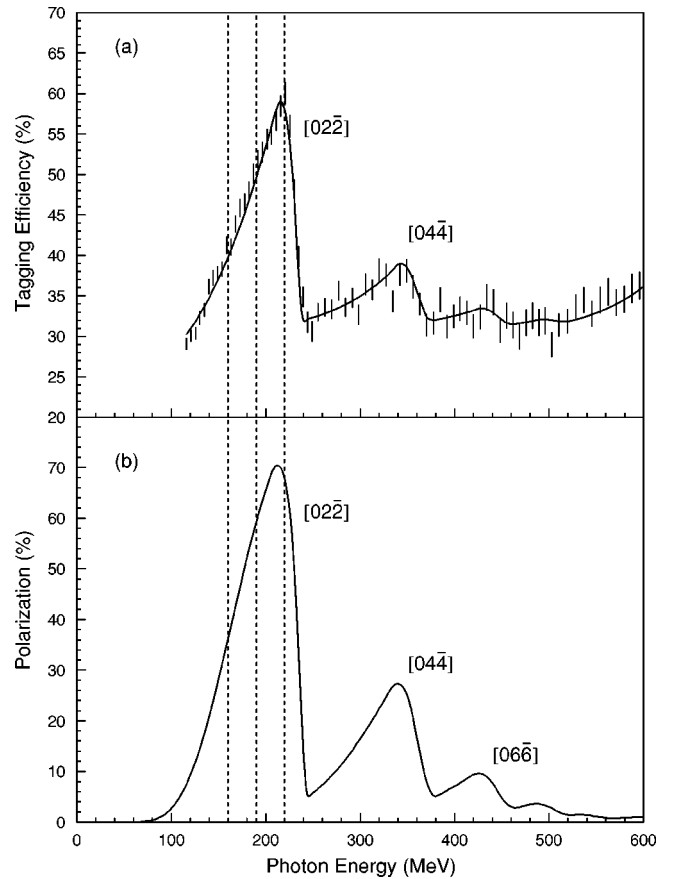


FIG. 2. (a) Tagging efficiency measurements from a diamond radiator for the lowest  $E_\gamma$  setting of the goniometer. The solid line is the result of the Monte Carlo code [26] described in the text. Peaks from the strongest reciprocal lattice vectors are labeled. The dashed lines show two of the  $E_\gamma$  bins used in the analysis. (b) The corresponding calculated photon polarization.

contribution amounted to  $\sim 3\%$  of the target-in yield and was subtracted in the data analysis. Details of the data acquisition, calibration, and particle selection techniques can be found in Refs. [13,23,24]. The  $E_m$  resolution was estimated to be  $\sim 8$  MeV from the width of the  $E_m$  peak in the  ${}^2\text{H}(\gamma, pn)$  calibration data. The resolution for  $(\gamma, pp)$  reactions is estimated to be similar.

The tagging efficiency ( $\epsilon_\gamma$ ), the fraction of tagged photons which pass through the collimator and hit the target, was measured periodically using a 30 radiation length Pb-glass detector with a low intensity beam. Figure 2(a) shows the measured  $\epsilon_\gamma$  for the lowest photon energy setting of the goniometer. The dashed vertical lines indicate the  $E_\gamma$  bins used in the data analysis. The strong  $E_\gamma$  dependence arises because the coherent bremsstrahlung has a much narrower angular distribution than the incoherent background and hence a larger fraction of the coherent photons pass through the collimator. The peaks in the tagging efficiency therefore correspond to regions of high photon polarization. The peak at  $\sim 200$  MeV is due mainly to the  $[02\bar{2}]$  reciprocal lattice vector with smaller contributions from higher order reciprocal lattice vectors evident at higher photon energies. A detailed study [25] showed no detectable difference in the  $\epsilon_\gamma$

spectra obtained with parallel or perpendicular photon polarization directions and Fig. 2(a) shows an average of the two orientations. The largest tagging efficiency measured was  $\sim 60\%$  for the lowest  $E_\gamma$  goniometer setting. For the two other settings it was  $\sim 54\%$  and  $\sim 50\%$ . The solid line is a calculation of  $\epsilon_\gamma$  produced by the same code used to calculate the photon polarization (see below). This gives excellent agreement with the measured tagging efficiency data.

Since the tagging efficiency and photon beam polarization depend strongly on the proper alignment and orientation of the incident electron beam, the diamond radiator and the collimator, two on-line diagnostics were employed to monitor the stability of the beam. The first was an image, obtained using a high sensitivity TV camera, of the light produced by a scintillator placed in the  $\gamma$  beam just in front of the beam dump. The position of the image is sensitive to the alignment (position and angle) of the electron beam at the radiator position. The second diagnostic was the position of the sharp falling edge on the high photon energy side of the photon polarization peak. This was observed using an on-line spectrum of hits in the tagger focal plane detector, normalized by an incoherent spectrum obtained using a nickel radiator. The position of the edge was very sensitive to both the diamond orientation and to the alignment of the incident electron beam. If any change was observed in either of these diagnostic monitors, the beam was realigned.

The polarization  $P$  of the photon beam was calculated using a Monte Carlo code [26] incorporating both the coherent and incoherent bremsstrahlung processes. The code takes into account the divergence of the incident electron beam, multiple scattering of the electron beam in the diamond radiator, thermal vibrations in the diamond and collimation of the photon beam. It includes the 20 strongest contributions from different sets of scattering planes in the diamond radiator.

Figure 2(b) shows the calculated photon polarization for the lowest photon energy goniometer setting. The peak at  $\sim 200$  MeV is due mainly to the  $[02\bar{2}]$  reciprocal lattice vector, although the polarization in this region also contains small contributions from the low-energy tails of many other reciprocal lattice vectors. In the data analysis two photon energy bins (denoted by dashed lines), with high values of photon polarization and tagging efficiency, were selected for each of the three goniometer settings. These regions were chosen on the low energy side of the polarization peak where the calculation of  $P$  is least sensitive to uncertainties in the parameters describing the electron beam and the diamond radiator. The six photon energy bins used for analysis were 160–190, 190–220, 220–250, 250–280, 290–320, and 320–350 MeV with average  $P$  values of 49.0%, 66.7%, 50.0%, 60.5%, 37.1%, and 49.5%, respectively.

The accuracy of the calculations was checked by comparing their predictions with measured collimated tagged photon energy spectra, obtained in “tagging efficiency” measurements. These comparisons gave very good descriptions of the data for all the crystal orientations used in this experiment [26]. The uncertainty of the calculated  $P$  values due to uncertainties in the input parameters was found to be less than  $\pm 0.02P$ . Making generous allowances for other pos-

sible sources of uncertainty, such as impurities in the diamond radiator, the overall systematic uncertainty in  $P$  is conservatively estimated to be less than  $\pm 0.05P$ . During the experiment no significant differences in the collimated photon energy spectra measured in tagging efficiency runs were detected between the “parallel” and “perpendicular” data sets and the difference between the photon polarizations for both orientations was estimated to be less than 1%.

There are several sources of possible systematic error in the experiment. Uncertainties in the detection of neutrons in TOF arise from the calculation of the neutron detection efficiency (10%) and from uncertainties in the TOF neutron detection thresholds (5%). The contribution to the charged particle yield in TOF due to neutral particles in random coincidence with signals from the  $\Delta E$  detectors near the target is generally small, except at the most forward angles where it can be as much as 10%. The TOF proton detection efficiency gives rise to an uncertainty of 3% in the TOF proton yield. The uncertainty in the PiP proton detection efficiency is 3%. Further uncertainties occur in the determination of the target thickness (1%) and the photon polarization (5%). Only uncertainties in the photon polarization affect the photon asymmetry data, shown in Figs. 4, 5, and 7, as the other factors affect the parallel and perpendicular data equally and cancel in the determination of  $\Sigma$ . The resulting uncertainty is  $\Delta\Sigma = 0.05\Sigma$ . Uncertainties in the factors, other than the photon polarization, combine to give systematic errors of 11% [10%] in the  $(\gamma, pn)$  [ $(\gamma, pp)$ ] yields and cross sections shown in Figs. 3 and 6. The uncertainty in the photon polarization has no effect on the average of the parallel and perpendicular cross sections, but does give rise to a systematic error of 5% in the difference between  $\sigma_{\parallel}$  and  $\sigma_{\perp}$ .

### III. THEORETICAL CALCULATIONS

The experimental results presented in this paper are compared with predictions of a direct two-nucleon knockout model developed by the Gent group [3]. Parallel and perpendicular cross sections and photon asymmetries are calculated from an unfactorized distorted wave treatment of the process. The model includes pion exchange and  $\Delta$ -isobar currents and incorporates central short-range correlations using a central correlation function  $f_c(r_{12})$  obtained from a  $G$ -matrix calculation by Gearhart and Dickhoff [27]. The effects of tensor correlations have also been included through the introduction of an operator  $f_{t\tau}(r_{12})\hat{S}_{12}$  which correlates all nucleon pairs. The strength of the tensor correlations is regulated by the correlation function  $f_{t\tau}(r_{12})$  for which the prediction from the variational  $^{16}\text{O}$  calculations by Pieper *et al.* [28] was used.

To average the calculations over the acceptance of the detectors a Monte Carlo technique developed by Ireland *et al.* [29] was used. This is necessary since significant variations in cross section can occur within relatively small angular bins and cross sections evaluated for the “central” kinematic conditions of a particular bin can be significantly different from the average over that bin. Similar effects are also seen in the calculation of  $\Sigma$ , but in this case the differ-

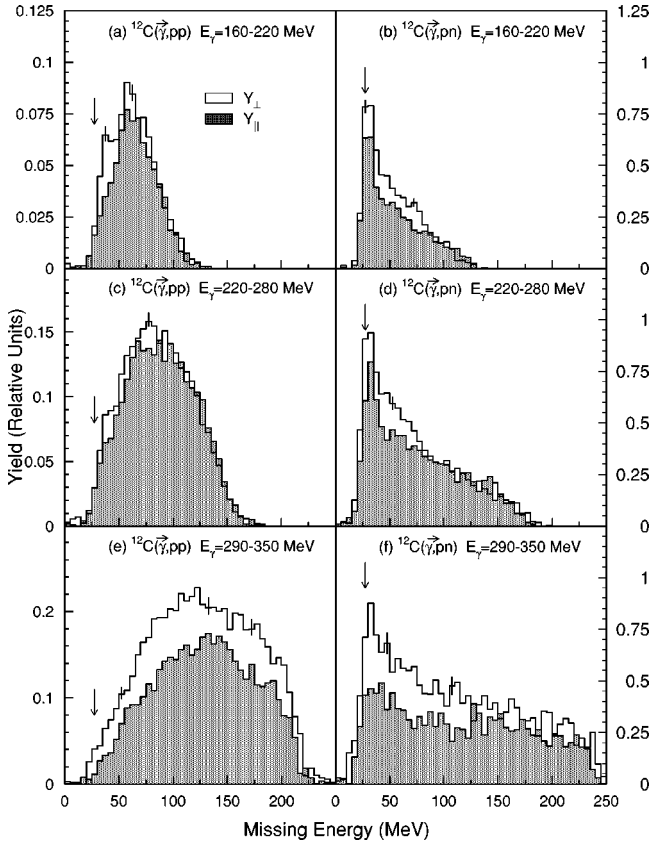


FIG. 3.  $^{12}\text{C}(\gamma,pp)$  and  $(\gamma,pn)$   $E_m$  spectra for photons polarized perpendicular (open) and parallel (shaded) to the detector plane. For clarity only a few sample error bars are shown. The arrows indicate the reaction thresholds.

ences between the average values and the central point values are generally small.

#### IV. RESULTS

Figure 3 shows the measured yield as a function of  $E_m$  for the  $(\vec{\gamma},pp)$  and  $(\vec{\gamma},pn)$  reactions on  $^{12}\text{C}$  for all the detected events. The experimental error bars represent the statistical uncertainties. Separate spectra are shown for data in which the photon polarization is parallel or perpendicular to the plane of the detectors. They show various features already established in previous work with unpolarized photons [13,30,31]. At low missing energies,  $E_m < 70$  MeV, where direct  $2N$  knockout is thought to be the main reaction mechanism, the  $(\gamma,pn)$  channel has a strong peak just above the reaction threshold in both  $Y_{\parallel}$  and  $Y_{\perp}$ . The  $(\gamma,pp)$  yield rises more slowly, but the shoulder at  $E_m \sim 40$  MeV in the two lowest photon energy ranges, first noted in the unpolarized work of Harty *et al.* [13], is now seen to be a distinct feature of  $Y_{\perp}$ . At higher  $E_m$  the spectra for both channels fall smoothly up to limits determined by the useful energy ranges of PiP and TOF.

The yields  $Y_{\parallel}$  and  $Y_{\perp}$  show clear differences. For the two lower photon energy ranges  $Y_{\perp}$  exceeds  $Y_{\parallel}$  in the region up to  $E_m \sim 80$  MeV, where direct two-nucleon emission is expected to play a major role, but there is little difference be-

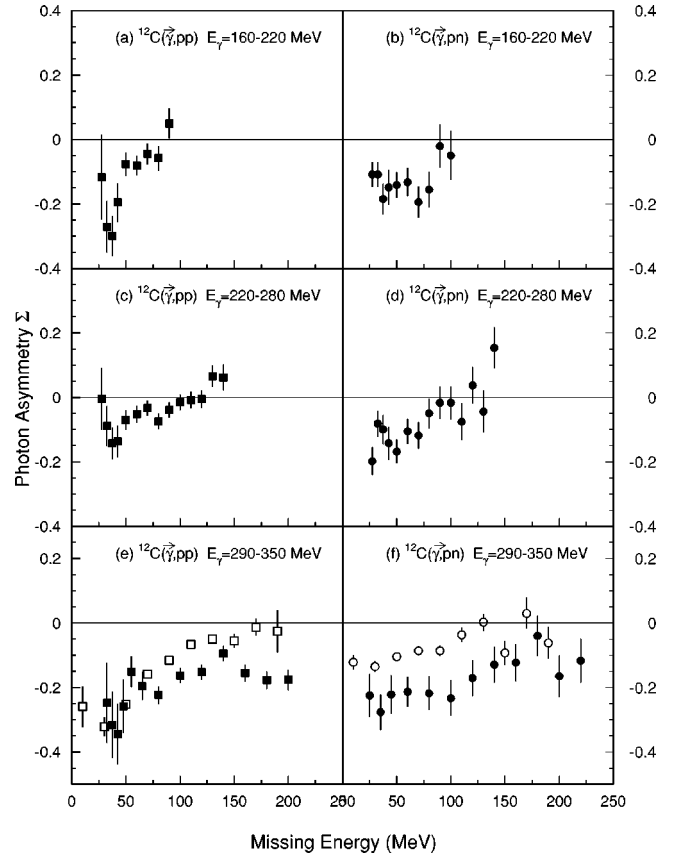


FIG. 4.  $\Sigma_{(\gamma,pp)}$  (solid squares) and  $\Sigma_{(\gamma,pn)}$  (solid circles) for  $^{12}\text{C}$  plotted as a function of  $E_m$ , for the same  $E_{\gamma}$  regions as Fig. 3. The open squares and circles are  $\Sigma_{(\gamma,pp)}$  and  $\Sigma_{(\gamma,pn)}$  for  $^{16}\text{O}$ ,  $E_{\gamma} = 285 - 315$  MeV [9].

tween them at higher  $E_m$ . In the highest photon energy range  $Y_{\perp}$  again exceeds  $Y_{\parallel}$ . However, the differences here are larger and persist, for both reaction channels, over the whole measured  $E_m$  range suggesting a different reaction mechanism in the  $\Delta$  resonance.

The photon asymmetry, derived from the data in Fig. 3, is shown in Fig. 4. The most striking observation is that  $\Sigma_{(\gamma,pp)}$  has a pronounced (negative) peak in all three  $E_{\gamma}$  ranges at low  $E_m \sim 40$  MeV where proton pair emission is expected from  $(1p)^2$  orbitals. The peak spreads to slightly higher  $E_m$  values in the higher  $E_{\gamma}$  ranges, perhaps due to the poorer nucleon energy resolution. Although the peak may be attributed to the shoulder in  $Y_{\perp}$  (see Fig. 3), the feature is more obvious in  $\Sigma_{(\gamma,pp)}$  and for the highest photon energy range is only visible in the asymmetry spectrum.

The magnitude of  $\Sigma_{(\gamma,pp)}$  at the peak tends to be greater than for  $\Sigma_{(\gamma,pn)}$  which shows a more gradual variation with  $E_m$ . These differences provide evidence for the direct  $2N$  knockout nature of the  $(\gamma,pp)$  process at least up to  $E_m \sim 50$  MeV, since a strong two-step contribution from an initial  $(\gamma,pn)$  reaction followed by charge exchange FSI would be expected to reduce slightly the initial asymmetry. They also tend to support the conclusion by Watts *et al.* [6] that different one- and two-body currents are important in the  $(\gamma,pp)$  and  $(\gamma,pn)$  processes at low  $E_m$ .

At higher  $E_m$  both  $\Sigma_{(\gamma,pp)}$  and  $\Sigma_{(\gamma,pn)}$  become smaller

and in the two lowest photon energy ranges tend toward zero, or even slightly positive values at the very highest  $E_m$ . In the highest photon energy range a different behavior is seen. The asymmetry for  $E_m > 100$  MeV stays fairly constant with roughly similar values, in the range  $-0.15$  to  $-0.20$ , for both channels. In this region both reaction channels are predicted to have large contributions from initial quasifree pion production followed by pion FSI [12], and the similarity in  $\Sigma$  values may reflect a common mechanism.

The  $^{12}\text{C}(\vec{\gamma}, pN)$   $\Sigma$  data for  $E_\gamma = 300\text{--}350$  MeV are also compared with recent  $^{16}\text{O}$  data obtained by the LEGS Collaboration [9,10] for  $E_\gamma = 285\text{--}315$  MeV. The LEGS data have poorer  $E_m$  resolution than the present data and the measurements are likely to be less sensitive to structure in the missing energy spectrum. The data were taken with more restrictive symmetric coplanar kinematics which emphasises contributions from  $\Delta$  currents. The  $\Sigma_{(\gamma,pp)}$  data for  $^{12}\text{C}$  and  $^{16}\text{O}$  are broadly similar below  $E_m \sim 100$  MeV, but at higher  $E_m$  the  $^{16}\text{O}$  data have a smaller magnitude. For the  $(\vec{\gamma}, pn)$  channel the  $^{16}\text{O}$  asymmetries are lower in magnitude than the present  $^{12}\text{C}$  data at all  $E_m$ . The comparison between these two data sets is discussed further below.

### A. Direct two-nucleon emission data

As shown by previous work with unpolarized photons [6,12,13,30] the contributing reaction mechanisms change rapidly with  $E_m$  for both the  $(\gamma, pn)$  and  $(\gamma, pp)$  reactions. At  $E_m < 40$  MeV the  $^{12}\text{C}$  data for both reaction channels are well described by a direct two-nucleon emission process in which both nucleons are ejected from  $(1p)$  orbitals. Between 40 and 70 MeV direct emission from  $(1p)(1s)$  orbitals predominates. Above 70 MeV more complex processes become important.

For further analysis, missing energy cuts of  $E_m < 40$  MeV and  $40 < E_m < 70$  MeV were applied to the data to emphasize direct two nucleon emission from  $(1p)^2$  and  $(1p)(1s)$  orbits, respectively. The separation of the two  $E_m$  regions is affected by the missing energy resolution, which worsens at higher photon energies, but the resultant error is less than  $\pm 0.015$  on measurements of  $\Sigma$  and less than  $\pm 4\%$  on the relative cross sections.

To ensure that the analyzed data sampled the peak of the direct  $(\gamma, NN)$  knockout angular correlation, and simultaneously reduced contributions from other processes, PiP and TOF angular bins were chosen on the basis of quasideuteron kinematics. Four TOF solid angle bins were used, *viz.* the two halves of TOF stands EF and GH, and the corresponding PiP solid angle bins were selected as described by Yau *et al.* [32].

#### 1. Photon energy dependence

Figure 5 shows the photon asymmetry for the two  $E_m$  regions as a function of  $E_\gamma$ , for data averaged over the four angular bins described above. The better statistical accuracy of the  $\Sigma_{(\gamma, pn)}$  is due to the larger  $(\gamma, pn)$  cross section. The small differences between the  $\Sigma_{(\gamma, pn)}$  results and the earlier

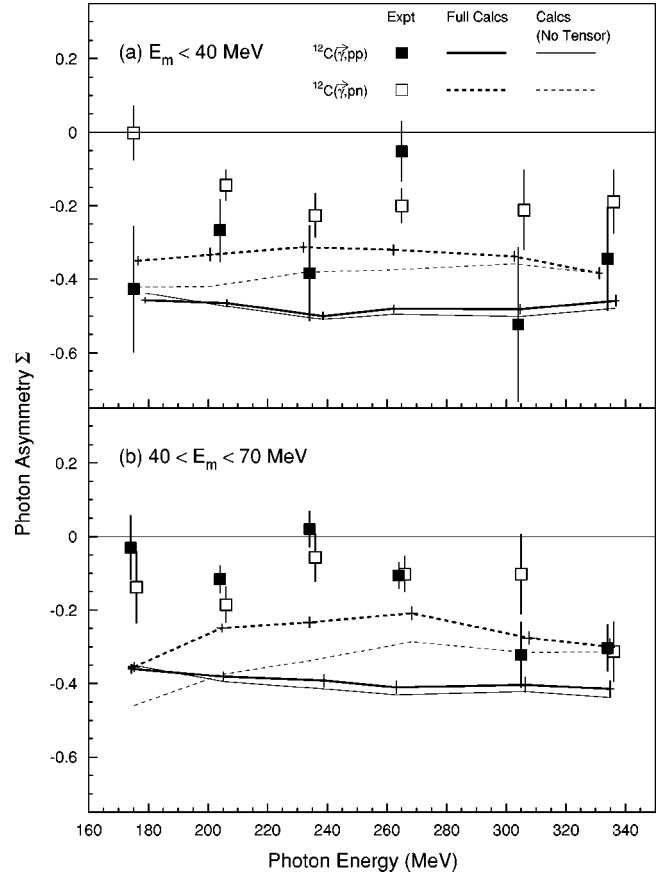


FIG. 5.  $\Sigma_{(\gamma, pp)}$  (solid squares) and  $\Sigma_{(\gamma, pn)}$  (open squares) for  $^{12}\text{C}$ , plotted as a function of  $E_\gamma$  and compared with two-nucleon emission calculations using the Gent model [3]. (a)  $E_m < 40$  MeV, (b)  $40 < E_m < 70$  MeV. Error bars on the calculations indicate the statistical uncertainty of sampling over the experimental data bins. Overlapping data points have been slightly displaced for the sake of clarity.

analysis reported in Ref. [15] are due to the different kinematic cuts used and the improved calculation of photon polarization.

For  $E_m < 40$  MeV, the magnitude of  $\Sigma_{(\gamma, pp)}$  is generally greater than  $\Sigma_{(\gamma, pn)}$ . In  $^{16}\text{O}$  MeV Lindgren *et al.* [9] observed that  $\Sigma_{(\gamma, pp)}$  was a factor of  $\sim 2.5$  greater than  $\Sigma_{(\gamma, pn)}$  for  $E_\gamma \sim 300$ . This factor is much larger than in  $^{12}\text{C}$  with the main difference being that  $\Sigma_{(\gamma, pn)}$  is appreciably smaller in  $^{16}\text{O}$  than in  $^{12}\text{C}$  (see Fig. 4). This may be due to the symmetric coplanar kinematic cuts imposed on the data in Ref. [9]. Franczuk *et al.* [15] compared  $\Sigma_{(\gamma, pn)}$  data with newer  $^{16}\text{O}$  data obtained in quasideuteron kinematics [14] and found no significant differences between  $^{16}\text{O}$  and  $^{12}\text{C}$ .

As discussed previously,  $\Sigma_{(\gamma, pp)}$  for coplanar kinematics in the factorized plane wave approximation, where it is assumed that the proton pair are in a relative  $S$  state, is expected to be  $\sim -1.0$ . The present  $^{12}\text{C}(\vec{\gamma}, pp)$  experiment satisfies this kinematic requirement but obtains  $\Sigma_{(\gamma, pp)}$  much smaller than  $-1$ . This is further evidence of the involvement of proton pairs in relative  $P$  and  $D$  states and demonstrates the need for calculations which take these contributions into

account. A similar conclusion was reached by Lindgren *et al.* [9] for  $^{16}\text{O}$ .

For  $40 < E_m < 70$  MeV, both  $\Sigma_{(\gamma,pp)}$  and  $\Sigma_{(\gamma,pn)}$  have small magnitudes for  $E_\gamma < 280$  MeV. The magnitude of  $\Sigma$  increases at higher photon energies in both reaction channels, perhaps indicating a change in reaction mechanism.

The data are compared with new calculations using the Gent model of two-nucleon emission from  $(1p_{3/2})^2$  orbitals for the low missing energy region, and  $(1p_{3/2})(1s_{1/2})$  orbitals for the higher missing energy region. The calculations do not do very well at predicting the magnitude and energy dependence of  $\Sigma$  for the two reaction channels.

In the low  $E_m$  region the calculations do predict that  $\Sigma_{(\gamma,pp)}$  is larger than  $\Sigma_{(\gamma,pn)}$  although the magnitude of the calculated asymmetry is greater than the experimental data for both reaction channels. The large negative asymmetry in the  $(\vec{\gamma},pp)$  channel is a reflection of the dominant role played by  $\Delta$  currents. The  $(\vec{\gamma},pn)$  channel, on the other hand, has additional contributions from MEC and the interference between the  $\Delta$  isobar and MEC amplitudes substantially reduces  $\Sigma_{(\gamma,pn)}$ . The  $E_\gamma$  dependence of the calculated  $\Sigma$  values is rather flat for both reaction channels, despite the fact that  $\Delta$ -current contributions are strongly energy dependent. In particular, the calculations do not reproduce the reduction in  $\Sigma_{(\gamma,pn)}$  at low  $E_\gamma$ .

The figure also shows the contribution from tensor correlations which predominantly affect proton-neutron pairs and have a significant influence on  $\Sigma_{(\gamma,pn)}$ , but hardly affect  $\Sigma_{(\gamma,pp)}$ . The inclusion of tensor correlations reduces the magnitude of  $\Sigma_{(\gamma,pn)}$ , bringing the calculations closer to the data.

For the higher  $E_m$  region, the calculated asymmetry is again generally larger than the experimental data. The effect of including tensor correlations is similar to the low  $E_m$  region. It reduces the magnitude of the  $\Sigma_{(\gamma,pn)}$  calculations but has little effect on  $\Sigma_{(\gamma,pp)}$ . It may be relevant that the calculations adopt the spectator approximation which implies that they do not account for multiple scattering processes involving other nucleons apart from the initial correlated pair. It is possible that the experimental data are affected to some extent by multiple scattering processes, especially in the region  $40 < E_m < 70$  MeV, which could reduce the asymmetries. The fact that the asymmetries tend to become smaller as  $E_\gamma$  decreases supports this suggestion.

## 2. Missing momentum dependence

Previous work with unpolarized photons [6,23,30] has shown that the variation of  $(\gamma,pp)$  and  $(\gamma,pn)$  cross sections with missing momentum depends on the angular momentum state of the initial pair. As  $\sigma_{\parallel}$  and  $\sigma_{\perp}$  are separately more sensitive to the angular momentum of the pair than unpolarized cross sections [1–3] the missing momentum dependence of the photon asymmetry was investigated.

For the low  $E_m$  region no significant variation in  $\Sigma_{(\gamma,pn)}$  with missing momentum was observed. The statistical accuracy of the low  $E_m$   $(\vec{\gamma},pp)$  data binned in this way was insufficient to allow any definite conclusions for  $\Sigma_{(\gamma,pp)}$  to be drawn. For the higher  $E_m$  region the data had better sta-

tistical accuracy and showed that the missing momentum dependence for both reaction channels is essentially flat. It is therefore reasonable to integrate over recoil momentum to investigate the dependence of polarization observables on other kinematic variables.

## 3. Angular dependence

Previous experimental work has shown that the  $^{12}\text{C}(\gamma,pp)$  and  $^{12}\text{C}(\gamma,pn)$  cross sections have a strong angular dependence [32]. Theoretical calculations [3] have predicted that polarization observables will also have a strong angular dependence. It is therefore of interest to look at the angular dependence of the present data. For this purpose the data were split into four TOF solid angle bins and parallel and perpendicular differential cross sections were evaluated. As the experiment was designed principally to measure the photon asymmetry the extracted cross sections have a relatively large systematic uncertainty and have been multiplied by a common normalization factor (1.5) to facilitate the comparison with the shapes of the theoretical distributions.

Both the observed and calculated angular distributions do show significant differences between  $\sigma_{\parallel}$  and  $\sigma_{\perp}$ , between  $(\vec{\gamma},pp)$  and  $(\vec{\gamma},pn)$  reaction channels, and between the two different missing energy regions. Figure 6 presents four typical examples of the angular dependence of the parallel and perpendicular cross sections plotted as a function of the polar angle of the nucleon detected in TOF. In general  $\sigma_{\perp}$  exceeds  $\sigma_{\parallel}$  at all angles and the two cross sections exhibit very different angular variations. The theoretical predictions for  $\sigma_{\parallel}$  and  $\sigma_{\perp}$  also show strong angular variations but these are more similar and do not correspond with the measured data. Similarly strong and different angular variations were observed in the eight spectra for other combinations of photon energy and missing energy for the two reactions channels which are not shown in Fig. 6, but no systematic variation was evident.

Although in principle studies of angular distributions will provide a sensitive test for calculations of two-nucleon emission, it is clear that improvements in the theoretical treatment and improved measurements, covering a wider range of angles with better accuracy, will both be required to provide a complete understanding of these processes.

## B. $E_m > 70$ MeV region

In the missing energy range above 70 MeV multistep processes are expected to dominate the cross section [6,12,13]. A comparison of missing energy spectra with calculations using the Valencia model [12] indicated that below  $E_\gamma \sim 250$  MeV the greatest contribution to this  $E_m$  region in both the  $(\gamma,pp)$  and  $(\gamma,pn)$  reactions is an initial photon absorption on a two-nucleon pair, followed by FSI. Above  $E_\gamma \sim 250$  MeV two-step processes involving pion production become important. In both reaction channels the most important process is then initial pion production on a nucleon followed by pion reabsorption on a pair of nucleons, although pion rescattering also contributes. The recoil momentum distributions for  $(\gamma,pp)$  and  $(\gamma,pn)$  reactions measured by Harty *et al.* [13] support these conclusions.

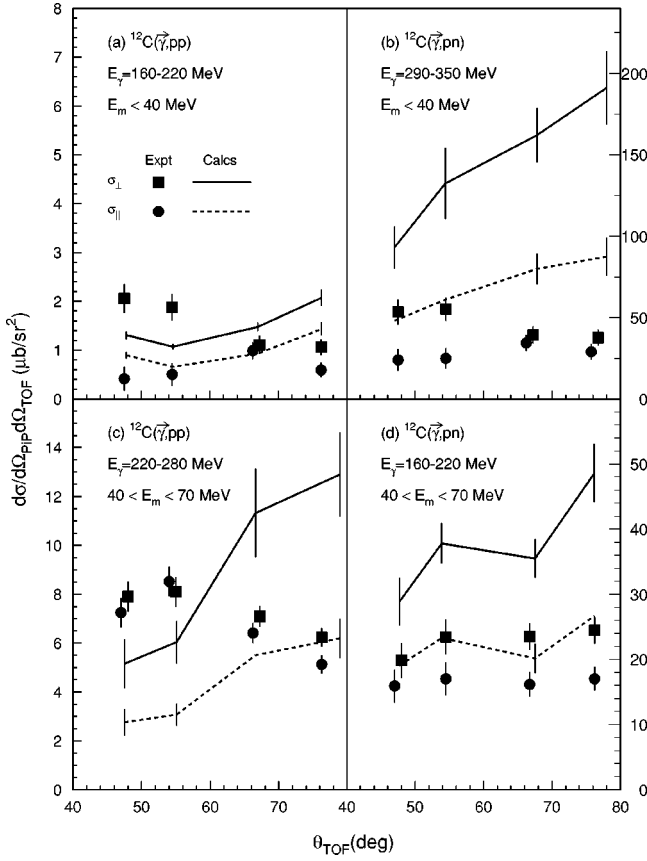


FIG. 6. Differential parallel and perpendicular cross sections for  $^{12}\text{C}(\gamma,pp)$  and  $(\gamma,pn)$  reactions as a function of  $\theta_{\text{TOF}}$ , for a sample of photon and missing energy ranges, compared with two-nucleon emission calculations using the Gent model [3]. The data have been normalized (see text) for comparison with the calculations. The scale relates to the theoretical cross sections. Error bars on the calculations are shown where they do not obscure the experimental data.

As the angular correlation between the nucleons emitted in two-step processes is much weaker than in direct two-nucleon emission, no angular cuts were made on the data for  $E_m > 70$  MeV. Figure 7 shows the photon energy dependence of  $\Sigma$ , averaged over the whole angular acceptance of PiP and TOF. The asymmetry is rather similar for both reaction channels as might be expected if the reactions are dominated by initial pion production. The asymmetry is small for  $E_\gamma < 270$  MeV but increases rapidly at higher energies. This may reflect the change from two-nucleon absorption followed by FSI to pion production followed by pion reabsorption as the  $\Delta$  resonance is approached.

The observed asymmetry in the  $(\vec{\gamma}, NN)$  reactions in the  $\Delta$ -resonance region may arise from the large asymmetry of an initial quasifree pion production process. It is known that pion production on the proton has large negative asymmetry values:  $\Sigma \sim -0.35$  for  $p(\vec{\gamma}, \pi^+)n$  and  $\Sigma \sim -0.45$  for  $p(\vec{\gamma}, \pi^0)p$  at  $E_\gamma \sim 300$  MeV [33]. The transfer of a large part of this asymmetry in pion reabsorption FSI is possible since the measured  $^2\text{H}(\pi^+, 2p)$  cross section is strongly peaked at forward-backward angles [34]. In addition to some reduction

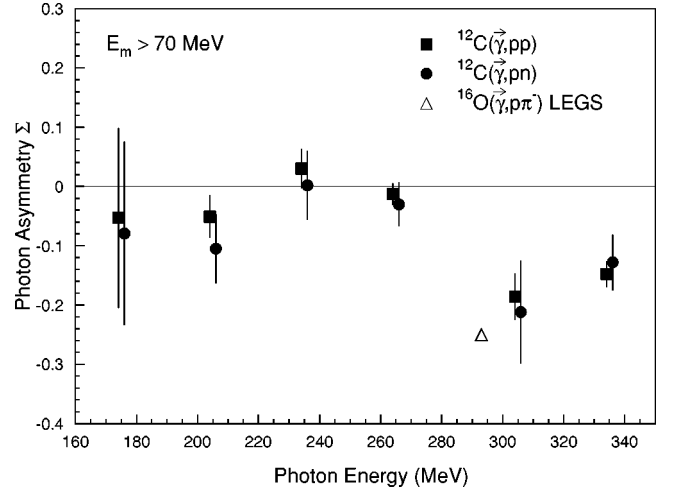


FIG. 7.  $\Sigma$  for  $^{12}\text{C}(\gamma,pp)$  (solid squares) and  $(\gamma,pn)$  (solid circles) reactions, for  $E_m > 70$  MeV, as a function of  $E_\gamma$ , compared with data from the  $^{16}\text{O}(\vec{\gamma}, \pi^- p)$  (open triangle) reaction [35].

in  $\Sigma$  due to FSI processes, the asymmetry of the initial process may be reduced in complex nuclei by Fermi motion of the nucleons involved. The present data are consistent with such an explanation although detailed modeling would be needed to substantiate this explanation.

However, the feedthrough of the strong asymmetry in the photopion production reactions on nucleons into the quasi-free photoproduction process in nuclei has already been seen in the  $^{16}\text{O}(\vec{\gamma}, \pi^- p)$  reaction [35] for which the asymmetry averaged over a wide angular range reaches the value  $\Sigma \sim -0.25$  for  $E_\gamma \sim 300$  MeV.

## V. SUMMARY

Measurements of the photon asymmetry for the  $^{12}\text{C}(\vec{\gamma}, pn)$  and  $(\vec{\gamma}, pp)$  reactions and its dependence on missing energy, nucleon knockout angle, and recoil momentum have been presented.  $\Sigma_{(\gamma,pp)}$  shows a peak and exceeds  $\Sigma_{(\gamma,pn)}$  at low missing energies where contributions from direct two-proton knockout are expected. This reinforces the conclusions of previous unpolarized photon work that this channel is dominated by a direct knockout mechanism at low  $E_m$ . It also supports the expectation that further planned studies of the  $(\gamma, pp)$  reaction [36] can provide information on SRC by selecting kinematic regions where the contribution from competing processes involving MEC or  $\Delta$  currents is suppressed.

No strong recoil momentum dependence of the photon asymmetry was established for either reaction channel within the limited statistical accuracy of the present data. In contrast the angular distribution data showed distinct differences between  $\sigma_\parallel$  and  $\sigma_\perp$ , for both reaction channels for  $E_m < 70$  MeV.

Two nucleon knockout calculations performed using the Gent unfactorized distorted wave two-nucleon knockout model provided a rather poor description of the present data. For  $(1p)^2$  emission they predict a stronger asymmetry for both  $(\vec{\gamma}, pn)$  and  $(\vec{\gamma}, pp)$  than observed experimentally and

do not show the observed fall in  $\Sigma_{(\gamma,pn)}$  at low photon energy. The calculated cross sections show strong angular variations in both reaction channels but again do not agree in detail with the data. A similar picture emerged for the comparison of  $(1p)(1s)$  emission calculations with the higher missing energy data.

For missing energies greater than 70 MeV, the observed asymmetries for both reaction channels are very similar. For  $E_\gamma < 270$  MeV, the asymmetry values are small and this is attributed to the strong contributions from two-step FSI processes, following initial photon absorption on a nucleon pair, which are expected at these energies. At higher photon energies two-step reactions involving initial quasifree pion production are believed to dominate. The experimentally observed asymmetries for both channels are reasonably strong  $\sim -0.18$  at  $E_\gamma \sim 320$  MeV. It is suggested that this may be due to a transfer of asymmetry from an initial quasifree pion production reaction to the final nucleon pair.

Overall this work has illustrated the importance of polarization observables in the study of photonuclear reactions. The new data already constrain theoretical models of direct two-nucleon emission and have also indicated other mechanisms at high missing energies. However, the present mea-

surements have limited statistical accuracy and energy resolution. Improvements in both are required for a detailed exploration of the dependence of the nuclear response to photon polarization and to study individual states in the residual nucleus. This is a necessary step to unravelling the strong angular momentum dependence of the polarization observables, glimpsed in the present limited angular distributions. There is also a need for measurements at higher photon energies and for other nuclei to investigate further the effects seen here.

## ACKNOWLEDGMENTS

This work was supported by the UK EPSRC, the British Council, the DFG (Mu 705/3, SSP 1043), BMFT (06 Tü 656), DAAD (313-ARC-IX-95/41), the EC [SCI.0910.C(JR)] and NATO (CRG 970268). The authors would like to thank the Institut für Kernphysik der Universität Mainz for the use of its facilities and for the generous assistance provided during the course of this experiment. C.J.Y.P, S.F., D.I.G., and J.F.A would like to thank EPSRC for research studentships during the period of this work.

- 
- [1] S. Boffi, C. Giusti, F. D. Pacati, and M. Radici, *Electromagnetic Response of Atomic Nuclei* (Oxford University Press, Oxford, 1996).
  - [2] C. Giusti and F. D. Pacati, Nucl. Phys. **A641**, 297 (1998).
  - [3] J. Ryckebusch *et al.*, Phys. Rev. C **57**, 1319 (1998); J. Ryckebusch *et al.*, Phys. Lett. B **291**, 213 (1992); L. Machenil *et al.*, *ibid.* **316**, 17 (1993); J. Ryckebusch *et al.*, Nucl. Phys. **A568**, 828 (1994); M. Vanderhaegen *et al.*, *ibid.* **A580**, 551 (1994).
  - [4] S. Boffi *et al.*, Nucl. Phys. **A564**, 473 (1993); C. Giusti *et al.*, *ibid.* **A546**, 607 (1992).
  - [5] P. Wilhelm, J. A. Niskanen, and H. Arenhövel, Nucl. Phys. **A597**, 613 (1996).
  - [6] D. P. Watts *et al.*, Phys. Rev. C **62**, 014616 (2000).
  - [7] D. J. Tedeschi *et al.*, Phys. Rev. Lett. **73**, 408 (1994).
  - [8] F. V. Adamian *et al.*, J. Phys. G **17**, 1657 (1991).
  - [9] R. Lindgren *et al.*, Report No. BNL-65187, <http://www.legs.bnl.gov/>
  - [10] H. Baghaei *et al.* (unpublished).
  - [11] A. M. Sandorfi *et al.*, Phys. Rev. C **53**, 1506 (1996).
  - [12] T. Lamparter *et al.*, Z. Phys. A **355**, 1 (1996).
  - [13] P. D. Harty *et al.*, Phys. Lett. B **380**, 247 (1996).
  - [14] V. Gladyshev, Ph.D thesis, University of Virginia, 1999.
  - [15] S. Franczuk *et al.*, Phys. Lett. B **450**, 332 (1999).
  - [16] S. J. Hall *et al.*, Nucl. Instrum. Methods Phys. Res. A **368**, 698 (1996); I. Anthony *et al.*, *ibid.* **301**, 230 (1991).
  - [17] H. Herminghaus (unpublished); T. Walcher, Prog. Part. Nucl. Phys. **24**, 189 (1990).
  - [18] D. Lohmann *et al.*, Nucl. Instrum. Methods Phys. Res. A **343**, 494 (1994).
  - [19] I. J. D. MacGregor *et al.*, Nucl. Instrum. Methods Phys. Res. A **382**, 479 (1996).
  - [20] A. Settele, Diploma thesis, University of Tübingen, 1996.
  - [21] P. Grabmayr *et al.*, Nucl. Instrum. Methods Phys. Res. A **402**, 85 (1998); T. Hehl *et al.*, *ibid.* **354**, 505 (1995).
  - [22] R. A. Cecil, B. D. Anderson, and R. Madey, Nucl. Instrum. Methods Phys. Res. A **161**, 439 (1979).
  - [23] I. J. D. MacGregor *et al.*, Phys. Rev. Lett. **80**, 245 (1998).
  - [24] J. R. M. Annand, I. Anthony, and B. Oussena, Nucl. Instrum. Methods Phys. Res. A **368**, 385 (1996); J. R. M. Annand and B. Oussena, *ibid.* **330**, 220 (1993).
  - [25] S. Franczuk, Ph.D. thesis, University of Glasgow, 1998.
  - [26] S. Wunderlich and F. A. Natter, internal report, 1998, University of Tübingen; F. A. Natter, in Proceedings of the 4th Workshop on Electromagnetically Induced Two-Hadron Emission, Granada, 1999, edited by C. Garcia-Recio, P. Grabmayr, A. M. Lallena, and R. O. Owens, pp. 59 and 60, <http://www.pit.physik.uni-tuebingen.de/grabmayr/CDgranada/>; F. A. Natter *et al.* (unpublished).
  - [27] C. C. Gearhart, Ph.D. thesis, University of Washington, 1994; W. Dickhoff (private communication).
  - [28] S. C. Pieper, R. B. Wiringa, and V. R. Pandahripande, Phys. Rev. C **46**, 1741 (1992).
  - [29] D. G. Ireland, I. J. D. MacGregor, and J. Ryckebusch, Phys. Rev. C **59**, 3297 (1999).
  - [30] J. C. McGeorge *et al.*, Phys. Rev. C **51**, 1967 (1995).
  - [31] S. N. Dancer *et al.*, Phys. Rev. Lett. **61**, 1170 (1988).
  - [32] T. T.-H. Yau *et al.*, Eur. Phys. J. A **1**, 241 (1998).
  - [33] F. A. Berends *et al.*, Nucl. Phys. **B4**, 54 (1967).
  - [34] H. J. Weyer, Phys. Rep. **195**, 295 (1990).
  - [35] K. Hicks *et al.*, Phys. Rev. C **55**, R12 (1997); **61**, 054609 (2000).
  - [36] I. J. D. MacGregor *et al.*, Mainz/Bonn PAC proposal A2/2-98, 1998; I. J. D. MacGregor, Proceedings of the 4th Workshop on Electromagnetically Induced Two-Hadron Emission, Granada, 1999 (Ref. [26]), pp. 339–352.